2024, 9(4s)

e-ISSN: 2468-4376

https://www.jisem-journal.com/

#### **Research Article**

# Damping Local Modes in Power Systems Using Frequency-Responsive Load Control

Chetna Sagar<sup>1</sup>, Ajit Kumar<sup>2</sup>

<sup>1</sup>Research Scholar, Electrical, NIT Patna, Patna, Bihar, India

<sup>2</sup> Doctor, Electrical, NIT Patna, Patna, Bihar, India; ajitk.ee@nitp.ac.in; https://orcid.org/0000-0002-1408-5450 \*Corresponding Author: chetnas.ph21.ee@nitp.ac.in; https://orcid.org/0000-0001-5199-2626

ARTICLE INFO	ABSTRACT
Received: 20 Oct 2024	This paper explores the role of load modeling in small-signal stability analysis, focusing on the
Revised: 22 Nov 2024	use of frequency-dependent static load (FDL) models. The study investigates the influence of FDLs on oscillation damping and the design of a locally measured power system stabilizer (PSS).
Accepted: 20 Dec 2024	A specific system configuration is considered, where the FDL is connected to the secondary bus of a step-up transformer. Both frequency domain and time domain analyses are conducted to assess the impact on system dynamics, with results demonstrated through eigenvalue evaluations and system responses to contingencies. The proposed modeling and control framework is validated using the IEEE 39-bus and 68-bus test systems, showing improved damping performance and enhanced small-signal stability.
	<b>Keywords:</b> Power system stability, power system stabilizer, frequency-dependent loads, local plant measurements.

#### INTRODUCTION

The dynamic behavior of power systems is significantly influenced by load characteristics, which act as a form of feedback within the system. Lightly damped or undamped low-frequency electromechanical oscillations (LFEOs) pose a serious challenge to system stability and may lead to large-scale power outages. These oscillations encompass intra-plant, local, and inter-area modes. Kundur et al. [1] demonstrated that while modern, high-gain, fast-acting excitation systems enhance the damping of inter-area modes, they may reduce the damping of local modes when compared to traditional low-gain excitation controllers. Several conventional strategies have been employed to mitigate LFEOs, including generation re-scheduling, deployment of power system stabilizers (PSS), auxiliary control for distributed energy resources, and supplementary damping controllers integrated into devices such as TCSC and SVC, as well as active power load modulation.

Although loads have a pronounced effect on power system stability [23]–[27], much of the existing research has primarily concentrated on generator and turbine control methods to mitigate LFEOs. However, various types of loads—such as voltage-dependent loads, frequency-dependent loads (FDLs), dynamic loads, and induction motor loads—can also play a significant role in influencing LFEO damping [25], [26], [28].

# A. Load Control for Damping Low-Frequency Electromechanical Oscillations

The use of load modulation as a means to damp low-frequency electromechanical oscillations (LFEOs) in power systems has been the subject of considerable research. Kamwa et al. [18] proposed a two-loop decentralized active power load modulation strategy to enhance system sstability, while Trudnowski [17] demonstrated that load modulation can also contribute to frequency regulation. However, applying active power modulation to control multiple inter-area oscillation modes can introduce significant computational complexity due to the need for coordination among numerous controllers [19].

Practical concerns also arise with respect to load modulation, particularly in scenarios involving substantial bus voltage oscillations, which may impair the effectiveness of certain loads [16], [21]. To address such limitations, Sabine et al. [26] introduced a method for smoothly modulating the power consumption of flexible demand-side loads

2024, 9(4s)

e-ISSN: 2468-4376

https://www.jisem-journal.com/

## **Research Article**

through voltage regulation, thereby improving the damping of inter-area oscillations. Nonetheless, Chao et al. [29] argued that this method may be impractical, as most real-world loads exhibit relatively slow response dynamics—typically in the range of several seconds to minutes.

While nonlinear adaptive decentralized controllers have been proposed to improve frequency stability [8], [14], [16], these approaches generally consider only the dynamics of locally connected frequency-dependent loads (FDLs) based on local measurements. Wide-area control schemes, though potentially more effective, are constrained by communication challenges, including latency, packet disorder, and synchronization issues [30]. Consequently, the power industry tends to favor simpler, more robust control strategies, such as proportional-integral-derivative (PID) and lead-lag controllers, due to their ease of implementation and proven reliability in practical settings [31].

Overall, the relatively low penetration of load-based control mechanisms in industrial applications can be attributed to a combination of factors, including consumer disutility, communication infrastructure limitations, and the complex and uncertain nature of load composition and behavior.

## B. Local Control for Damping Low-Frequency Electromechanical Oscillations

Local control strategies for damping low-frequency electromechanical oscillations (LFEOs) have gained attention due to their practicality and reduced reliance on wide-area communication. Lam et al. [32] introduced a power system stabilizer (PSS) design framework based on local measurements by decomposing the generator's frequency response into two distinct components. The first component, which depends solely on the associated generator, has a dominant influence on the overall frequency response and remains robust under varying operating conditions. The second component, which incorporates interactions with the external network, is comparatively weaker due to the diagonal dominance of the reduced admittance matrix. These insights form the theoretical foundation for several PSS designs based on local plant signals, as explored in [3]–[11].

Gibbard et al. [3] demonstrated that the P-Vr-type PSS offers robust performance, largely invariant to the characteristics of individual generators—an observation supported by Lam's theoretical analysis. Building on this foundation, Gurrala et al. [4] proposed a PSS design utilizing local plant signals up to the secondary bus of the step-up transformer. Kumar [6] extended this approach by designing a PSS based on signals originating directly from the secondary side of the step-up transformer. Further developments have applied similar local control strategies in the context of microgrids [10] and the Indian power grid [8].

Marco et al. [5] introduced a low-computation phase-shaping technique for PSS design in multi-machine systems, arguing that Lam's findings justify the use of the single-machine infinite bus (SMIB) model for effective PSS design in such environments. In addition, advanced local control techniques such as feedback linearization [33] and energy-dissipating hybrid controllers [11] have also been developed, leveraging local plant measurements to enhance damping and system stability.

#### **OBJECTIVES**

The influence of nearby loads on power system stability—particularly in contrast to distant loads—has been well documented in the literature [24], [26], [34]. Notably, frequency-dependent loads (FDLs) situated close to generators have been shown to increase the diagonal dominance of the reduced admittance matrix, thereby exerting a significant influence on the frequency response of the associated generators [32]. To account for this effect, we extend the generator modeling approach proposed in [6] by incorporating the dynamic behavior of FDLs connected to the secondary bus of the step-up transformer, which is electrically close to the generator terminals. In the IEEE 39-bus and 68-bus test systems, four and eight major loads, respectively, are connected at these secondary buses, providing a realistic framework to evaluate the impact of local FDLs on system dynamics.

# The primary contributions of this paper are as follows:

- 1. The single-generator plant model proposed in [6] is extended to include the dynamics of FDLs connected to the secondary bus of the generator's step-up transformer.
- 2. The impact of FDLs on system stability is analyzed through the modification of the open-loop plant transfer function, highlighting changes in frequency response and eigenvalue behavior.

2024, 9(4s)

e-ISSN: 2468-4376

https://www.jisem-journal.com/

## **Research Article**

3. A conventional lead-lag power system stabilizer (PSS) is designed based on the modified plant model, and its performance is evaluated across a wide range of operating conditions through both frequency-domain and time-domain analyses.

TABLE I PSS AND WADC DATA,  $T_w = 10$ 

Sl.No.	Kumar [6]	Kamwa	Ref. [20]
		[38]	
PSS#1	30.8	30	10
PSS#2	19	30	_
PSS#3	23	30	10
PSS#4	27	30	_
WADC#1	_	_	0.66
WADC#2	_	_	0.68

Kumar [6]:  $T_1 = 0.1732, T_2 = 0.0577, T_3 = T_4 = 0$ 

Kamwa [20], [38]:  $T_1 = 0.05, T_2 = 0.02, T_3 = 3, T_4 = 5.4$ 

WADC#1:  $T_5 = 0.32, T_6 = 0.1$ ; WADC#2:  $T_5 = 0.27, T_6 = 0.1$ 

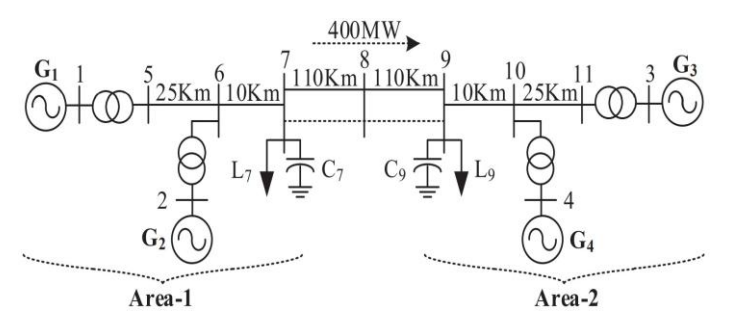


Fig. 1. Single line diagram of 4-machine 11-bus system.

The PSS designed using proposed technique have shown enhanced rotor mode damping in contrast with PSS designed in [6], [35], [36], over a wide range of operating secanrios. To demonstrate the efficacy of the proposed method, two IEEE test models are considered i) 39 bus and ii) 68 bus power system.

# **Comparison of Wide-Area and Local-Area Damping Controllers**

To compare the effectiveness of wide-area and local-area damping controllers, Kundur's two-area benchmark system [37] is utilized. Following the methodology outlined in [20], a wide-area damping controller (WADC) is implemented through the modulation of active power demand. In this approach, particle swarm optimization (PSO) is employed to design the WADCs at Load 1 and Load 2.

The transfer functions of both the power system stabilizers (PSSs) and the WADCs used in this study are provided below to facilitate direct performance comparison.

$$H_{PSS}(s) = K_L \frac{sT_w}{1 + sT_w} \frac{1 + sT_1}{1 + sT_2} \frac{1 + sT_3}{1 + sT_4}$$
 (1)

$$H_{WADC}(s) = K_W \frac{sT_w}{1 + sT_w} \frac{1 + sT_5}{1 + sT_6}$$
 (2)

where  $K_L$  and  $K_W$  are PSS and WADC gains. PSSs and WADCs data are given in Table. I.

2024, 9(4s)

e-ISSN: 2468-4376

https://www.jisem-journal.com/

### **Research Article**

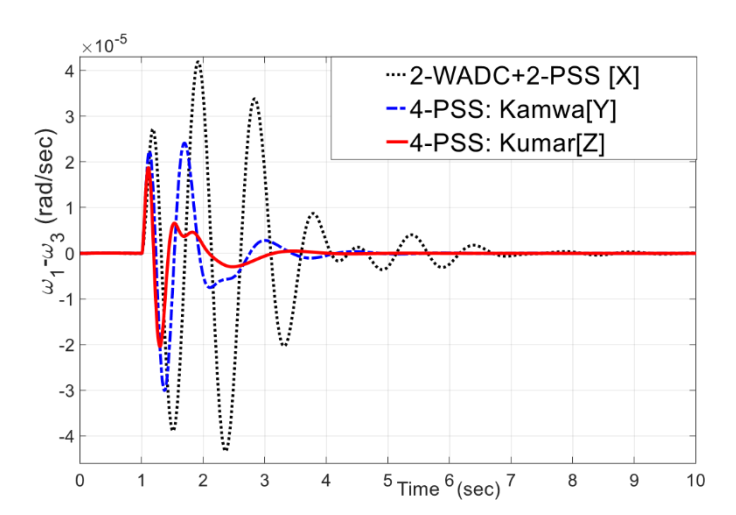


Fig. 2. Slip speed for Gen#1 w.r.t. Gen#3, for a change in  $V_{ref}$  at Gen-1 by 0.05 pu for 100ms. X= [20], Y= [38], Z= [6].

In reference [38], Kamwa et al. designed a power system stabilizer (PSS) for a two-area power system. Building on the approach presented by Kumar [6], we design a PSS using local measurements. The PSS gains are selected as one-fifth of the critical gain, as recommended in [39].

Figure 2 illustrates the slip speed response of Generator 1 (Gen-1) with respect to Generator 3 (Gen-3) for a change in the reference voltage (Vref) at Gen-1 by 0.05 p.u. over a 100 ms period. As observed, the system damping performance with the PSS proposed in [6] outperforms the wide-area damping controllers (WADCs) and PSSs used in [20]. Specifically, a well-tuned PSS designed using local measurements demonstrates superior damping performance compared to the WADCs.

Motivated by these results, the PSS design in [6] is further refined by incorporating frequency-dependent loads (FDLs) connected nearby, utilizing local measurements to enhance the damping performance.

# **METHODS**

# **Power System Model**

In power system studies, a third-order synchronous machine model, represented as the voltage behind the direct-axis transient reactance, is commonly employed for designing excitation controllers [40]. It is important to note that low-order control schemes are preferred in industrial practice due to their reliability, robustness, and the extensive expertise available for their implementation. The dynamic equations for the i-th machine, which are suitable for excitation control, can be expressed as follows:

$$\dot{\mathcal{S}}^i = \omega_{\scriptscriptstyle R} S_{\scriptscriptstyle m}^i \tag{3}$$

$$2H^{i}\dot{S}_{m}^{i} = T_{m}^{i} - T_{e}^{i} - D^{i}S_{m}^{i} \tag{4}$$

$$T_{do}^{\prime i} \dot{E}_{q}^{\prime i} = -E_{q}^{i} + (X_{d}^{i} - X_{d}^{\prime i}) I_{d}^{i} + E_{fd}^{\prime}$$
(5)

where,

$$T_e^i = E_q^{\prime i} I_q^i + (X_d^{\prime i} - X_q^i) I_q^i I_d^i$$
 (6)

The stator equations of *i*<sup>th</sup> generator in the algebraic form are given as

$$E_{q}^{\prime i} + X_{d}^{\prime i} I_{d}^{i} - R_{a}^{i} I_{q}^{i} = V_{q}^{i} \tag{7}$$

2024, 9(4s)

e-ISSN: 2468-4376

https://www.jisem-journal.com/

#### **Research Article**

$$-X_a^i I_a^i - R_a^i I_d^i = V_d^i \tag{8}$$

$$V_t^i = \sqrt{(V_q^i)^2 + (V_d^i)^2} \tag{9}$$

The variables used in this section employ conventional notations [41]. The rotor angle with respect to the secondary voltage bus of transformer  $(V_s^i \angle \theta_s^i)$  is denoted as  $\delta_s^i = \delta^i - \theta_s^i$ .

Using local measurements, the rotor angle  $\delta_s^i$  and  $E_q^{\prime i}$  are given as follows

$$\delta_{s}^{i} = \delta^{i} - \theta_{s}^{i} = tan^{-1} \frac{P_{s}^{i} X_{qt}^{i} - Q_{s}^{i} R_{t}^{i}}{P_{s}^{i} R_{t}^{i} + Q_{s}^{i} X_{qt}^{i} + (V_{s}^{i})^{2}}$$
(10)

$$E_q^{ii} = \frac{X_{dt}^{ii}}{X_t^i} \sqrt{(V_t^i)^2 - \frac{(X_q^i V_s^i \sin \delta_s^i)^2}{(X_{qt}^i)^2}} - \frac{X_d^{ii} V_s^i \cos \delta_s^i}{X_t^i}$$
(11)

where,  $X_{qt}^i = X_q^i + X_t^i$ ,  $X_{dt}^{ii} = X_d^{ii} + X_t^i$ ,  $X_{qt}^{ii} = X_q^{ii} + X_t^i$ .  $P_s^i = V_s^i I_a^i \cos \theta_p^i$ ,  $Q_s^i = V_s^i I_a^i \sin \theta_p^i$  is power factor angle at the high voltage bus.  $V_s^i$  and  $\theta_s^i$  are the magnitude and angle of the secondary bus of the transformer respectively. The expressions for  $I_d^i$ ,  $I_q^i$ ,  $V_d^i$  and  $V_q^i$  are given as follow:

$$I_{d}^{i} = \frac{V_{s}^{i} \cos \delta s^{i} - E_{q}^{'i}}{X_{dt}^{'i}} \; ; \; I_{q}^{i} = \frac{V_{s}^{i} \sin \delta_{s}^{i}}{X_{qt}^{i}}$$
 (12)

$$V_{q}^{i} = \frac{X_{t}^{i}}{X_{dt}^{'i}} E_{q}^{'i} + \frac{X_{d}^{'i}}{X_{dt}^{'i}} V_{s}^{i} \cos \delta_{s}^{i}; V_{d}^{i} = -\frac{X_{q}^{i}}{X_{at}^{i}} V_{s}^{i} \sin \delta_{s}^{i}$$
(13)

Locally procurable data  $Z_{ei}(R_{ei}+jX_{ei})$  for the  $i^{th}$  transmission line originating from the secondary bus of stepup transformer are used to evaluate  $E_{bi}$  and  $\alpha_i = \theta_s - \theta_i$ , [6] they are given as:

$$\alpha_{i} = tan^{-1} \frac{P_{si} X_{ei} - Q_{si} R_{ei}}{V_{s}^{2} - P_{si} R_{ei} - Q_{si} X_{ei}}$$
(14)

$$E_{bi} = V_s \cos \alpha_i - I_i (R_{ei} \cos \beta_i + X_{ei} \sin \beta_i)$$
(15)

where  $P_{si} = V_s I_i \cos \theta_{si}$ ,  $Q_{si} = V_s I_i \sin \theta_{si}$  and  $\beta_i = \theta_{si} - \alpha_i \cdot \theta_{si}$  is the power factor angle at the high voltage bus w.r.t.  $I_i$ . From above relationships, equivalent bus voltage  $E_b$ ,  $\delta_b - \theta_b$  and  $X_e$  are given below and used in Fig. 5.

$$E_{b} = X_{e} \sqrt{\sum_{j=1}^{n} \sum_{i=1}^{n} \frac{E_{bj}}{X_{ej}}} \frac{E_{bi}}{X_{ei}} \cos(\alpha_{i} - \alpha_{j})$$

$$X_{e} = X_{e1} X_{e2} (X_{e2} + X_{e1})^{-1}$$

$$\delta_{b} = \delta - \theta_{b} = \tan^{-1} \left( \frac{\sum_{i=1}^{n} E_{bi} X_{ei}^{-1} \sin(\delta_{s} + \alpha_{i})}{\sum_{i=1}^{n} E_{bi} X_{ei}^{-1} \cos(\delta_{s} + \alpha_{i})} \right)$$
(16)

2024, 9(4s)

e-ISSN: 2468-4376

https://www.jisem-journal.com/

# **Research Article**

## TABLE II TYPICAL LOAD FREQUENCY DEPENDENCE PARAMETER.

Load Type	kpf	kqf
Water Heater	0	-2.3
3-phase Air conditioner	0.98	-1.8
Fan motors	2.9	1.8
Agriculter pump	5.6	4.2
	/ 2 Г . а Т	

unit of  $K_{pf}$ ,  $K_{qf}$  is 'pu/pu' [42].

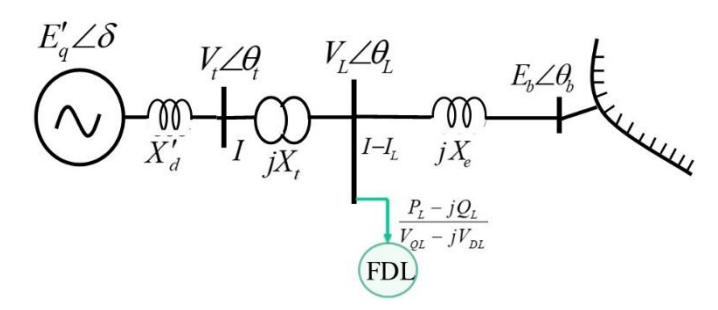


Fig. 3. A single machine in a connected network [6] with FDL.

# FREQUENCY DEPENDENT NONLINEAR LOAD

In Table II, presents the active and reactive power load frequency dependence values for various types of loads [40],[43]. Real and imaginary power of the nonlinear load is written below. The active power can be expressed as:

$$P_{L} = P_{L0}c_{1}\left(\frac{V_{L}}{V_{L0}}\right)^{m_{p1}}\left(1 + k_{pf}(f - f_{0})\right) + P_{L0}\left(1 - c_{1}\right)\left(\frac{V_{L}}{V_{L0}}\right)^{m_{p2}}$$
(17)

Taking  $c_1 = 1$  and  $m_{p1}$  and  $m_{p2}$  as 0, (17) becomes as:

$$P_{L} = P_{L0} \left( 1 + k_{pf} (f - f_{0}) \right) \tag{18}$$

Where,  $f - f_0$  is the frequency deviation from the nominal.

The reactive power can be expressed as:

$$\frac{Q_L}{P_{L0}} = c_2 \left(\frac{V_L}{V_{L0}}\right)^{m_{q1}} \left(1 + k_{pf}(f - f_0)\right) + \left(\frac{Q_{L0}}{P_{L0}} - c_2\right) \left(\frac{V_L}{V_{L0}}\right)^{m_{q2}} \left(1 + k_{qf}(f - f_0)\right)$$
(19)

Where,  $f-f_0$  is the frequency deviation from the nominal.

Taking  $c_2 = 0$  and  $m_{q1}$  and  $m_{q2}$  as 0, (19) becomes as:

$$Q_{L} = Q_{L0} \left( 1 + k_{qf} (f - f_{o}) \right) \tag{20}$$

2024, 9(4s)

e-ISSN: 2468-4376

https://www.jisem-journal.com/

#### **Research Article**

Where,  $f - f_0$  is the frequency deviation from the nominal.

The impact of only frequency dependency is observed by setting  $k_{\it pf}$ ,  $k_{\it qf}$  as -1, 0 and 1 respectively.

In Kron's frame of reference, load current  $\,I_{\scriptscriptstyle L}\,$  can be given as:

$$I_{L} = I_{QL} + jI_{DL} = \frac{P_{L} - jQ_{L}}{conj(\hat{V}_{L})} = \frac{P_{L} - jQ_{L}}{V_{L}^{2}} \hat{V}_{L}$$
(21)

It can be further expressed as:

$$I_{L} = \frac{P_{L0} - jQ_{0}}{V_{L}^{2}} \hat{V}_{L} + \frac{\left(P_{0}k_{pf} - jQ_{0}k_{qf}\right)\left(f - f_{0}\right)}{V_{L}^{2}} \hat{V}_{L}$$
(22)

# SMALL SIGNAL ANALYSIS OF SYSTEM

In a SMIB power system model. The stator algebraic equations with respect to load bus  $(V_t \angle \theta_t)$  are as follows:

$$V_{a} = X_{d}'I_{d} + E_{a}' \tag{23}$$

$$V_d = -X_a I_a \tag{24}$$

The stator algebraic equations with respect to load bus  $(V_L \angle \theta_L)$  are as follows:

$$\mathbf{E'}_{a} + \mathbf{X'}_{dt} \mathbf{I}_{d} = \mathbf{V}_{aL} \tag{25}$$

$$-X_{at}I_{a}=V_{dL}$$
 (26)

Where,  $X'_{dt} = X'_{d} + X_{t}$ ;  $X_{qt} = X_{q} + X_{t}$ .

Linearizing (25) and (26), we get:

$$\Delta E_a' + X_{dt}' \Delta I_d = \Delta V_{al} \tag{27}$$

$$-X_{qt}\Delta I_q = \Delta V_{dL} \tag{28}$$

The complex terminal voltage  $(V_I \angle \theta_I)$  in the Fig. 5, can be written as:

$$V_{L} \angle \theta_{L} = V_{L} e^{\angle \theta_{L}} = V_{QL} + j V_{DL} = \left(V_{qL} + j V_{dL}\right) e^{j\delta}$$

$$= j X_{e} \left(I_{q} + j I_{d} - I_{qL} - j I_{dL}\right) e^{j\delta} + E_{b} \angle \theta_{b}$$

$$(29)$$

Splitting up into real and imaginary parts, we get:

$$V_{aL} = -X_e I_d + X_e I_{dL} + E_b \cos \delta_b \tag{30}$$

$$V_{dL} = X_e I_a - X_e I_{aL} - E_b \sin \delta_b \tag{31}$$

where,  $\delta_b = \delta - \theta_b$ 

Thereafter, linearizing (30) and (31) for a given operating condition, we get:

2024, 9(4s)

e-ISSN: 2468-4376

https://www.jisem-journal.com/

#### **Research Article**

$$\Delta V_{aI} = -X_{e}\Delta I_{d} + X_{e}\Delta I_{dI} - E_{h}\sin\delta_{h0}\Delta\delta_{h}$$
 (32)

$$\Delta V_{dL} = X_e \Delta I_a - X_e \Delta I_{aL} - \Delta E_b \cos \delta_{b0} \Delta \delta_b \tag{33}$$

Linearizing secondary bus voltage of the step up transformer  $(V_L \angle \theta_L)$  in park's frame of reference, we get:

$$\Delta V_{L} = \frac{V_{qL0}}{V_{L0}} \Delta V_{qL} + j \frac{V_{dL0}}{V_{L0}} \Delta V_{dL}$$
(34)

At a nominal operating condition,  $(V_L \angle \theta_L)$  can be written as:

$$\hat{V}_{L0} = V_{L0} \left( \cos \theta_{L0} + j \sin \theta_{L0} \right) \tag{35}$$

Next linearizing (22),  $\Delta I_L$  can be expressed as:

$$\Delta I_{L} = \left(\frac{P_{L0} - jQ_{L0}}{V_{L0}^{2}}\right) \Delta \hat{V_{L}} - 2\left(\frac{P_{L0} - jQ_{L0}}{V_{L0}^{3}}\right) \Delta V_{L} \hat{V_{L0}} + \left(\frac{P_{L0}k_{pf} - jQ_{L0}k_{qf}}{V_{L0}^{2}}\right) \hat{V_{L0}} \Delta f$$
(36)

After further simplifications, (36) is given as:

$$\Delta I_{L} = (G_{L0} + jB_{L0})(\Delta V_{qL} + j\Delta V_{dL})$$

$$-2\left(\frac{P_{L0} - jQ_{L0}}{V_{L0}^{2}}\right)(\cos\theta_{L0} + j\sin\theta_{L0})\left(\frac{V_{dL0}}{V_{L0}}\Delta V_{dL} + \frac{V_{qL0}}{V_{L0}}\Delta V_{qL}\right)$$

$$+\left(\frac{P_{L0}k_{pf} - jQ_{L0}k_{qf}}{V_{L0}}\right)(\cos\theta_{L0} + j\sin\theta_{L0})\Delta f$$
(37)

Where,

$$G_{L0} = \frac{P_{L0}}{V_{L0}^2}, B_{L0} = -\frac{Q_{L0}}{V_{L0}^2}$$

$$G' = -2\frac{P_{L0}\cos\theta_{L0} + Q_{L0}\sin\theta_{L0}}{V_{L0}^2}$$

$$B' = -2\frac{P_{L0}\sin\theta_{L0} - Q_{L0}\cos\theta_{L0}}{V_{L0}^2}$$

$$B_1 = B'\frac{V_{qL0}}{V_{L0}}, B_2 = -G'\frac{V_{dL0}}{V_{L0}},$$

$$G_1 = B'\frac{V_{dL0}}{V_{L0}}, G_2 = G'\frac{V_{qL0}}{V_{L0}}$$

2024, 9(4s)

e-ISSN: 2468-4376

https://www.jisem-journal.com/

#### **Research Article**

$$\begin{split} F_{R} &= \frac{P_{L0} k_{pf} \cos \theta_{L0} + Q_{L0} k_{qf} \sin \theta_{L0}}{V_{L0}} \\ F_{I} &= \frac{P_{L0} k_{pf} \sin \theta_{L0} - Q_{L0} k_{qf} \cos \theta_{L0}}{V_{L0}} \end{split}$$

After further simplifications, we get the followings:

$$\Delta I_{qL} = (G_{L0} + G_2)\Delta V_{qL} - (B_{L0} + B_2)\Delta V_{dL} + F_R \Delta f$$
 (38)

$$\Delta I_{dL} = (B_{L0} + B_1) \Delta V_{dL} + (G_{L0} + G_1) \Delta V_{dL} + F_I \Delta f \tag{39}$$

After little algebraic manipulation in (32) and (33) respectively,  $\Delta V_{aL}$  and  $\Delta V_{dL}$  can be written as:

$$\Delta V_{qL} (1 - X_e (B_{L0} + B_1)) = -X_e \Delta I_d +$$

$$X_e (G_{L0} + G_1) \Delta V_{dL} + X_e F_I \Delta f - E_b \sin \delta_{b0} \Delta \delta_b$$

$$\Delta V_{dL} (1 - X_e (B_{L0} + B_2)) = X_e \Delta I_q - X_e (G_{L0} + G_2) \Delta V_{qL}$$

$$-X_e F_R \Delta f - E_b \cos \delta_{b0} \Delta \delta_b$$
(40)

Using  $\Delta V_{qL}$  and  $\Delta V_{dL}$  from (27) and (28) respectively, aforementioned equations can be given as:

$$\zeta_{1}\left(\Delta E_{q}' + X_{dt}'\Delta I_{d}\right) = -X_{e}\Delta I_{d} + X_{e}(G_{L0} + G_{1})\Delta V_{dL} 
+ X_{e}F_{I}\Delta f - E_{b}\sin\delta_{b0}\Delta\delta_{b} 
- \zeta_{2}X_{qt}\Delta I_{q} = X_{e}\Delta I_{q} - X_{e}(G_{L0} + G_{2})\left(\Delta E_{q}' + X_{dt}'\Delta I_{d}\right) 
- X_{e}F_{R}\Delta f - E_{b}\cos\delta_{b0}\Delta\delta_{b}$$
(42)

where, 
$$\zeta_1 = 1 - X_e \left( B_{L0} + B_1 \right), \zeta_2 = 1 - X_e \left( B_{L0} + B_2 \right)$$

Re-arranging (42) and (43), we obtain:

$$\begin{bmatrix} \zeta_1 X'_{dt} + X_e & X_e (G_{L0} + G_1) X_{qt} \\ X_e X'_{dt} (G_{L0} + G_2) & -X_e - \zeta_2 X_{qt} \end{bmatrix} \begin{bmatrix} \Delta I_d \\ \Delta I_q \end{bmatrix} = \\ \begin{bmatrix} X_e F_I & -E_b \sin \delta_{b0} & -\zeta_1 \\ -X_e F_R & -E_b \cos \delta_{b0} & -X_e (G_{L0} + G_2) \end{bmatrix} \begin{bmatrix} \Delta f \\ \Delta \delta \\ \Delta E'_q \end{bmatrix}$$

Simplifying the above matrix, we have

$$\begin{bmatrix} \Delta I_d \\ \Delta I_q \end{bmatrix} = \frac{-1}{A_f} \begin{bmatrix} X_e + \zeta_2 X_{qt} & X_e (G_{L0} + G_1) X_{qt} \\ X_e X'_{dt} (G_{L0} + G_2) & -(\zeta_1 X'_{dt} + X_e) \end{bmatrix} \begin{bmatrix} -X_e F_I & E_b \sin \delta_{b0} & \zeta_1 \\ X_e F_R & E_b \cos \delta_{b0} & X_e (G_{L0} + G_2) \end{bmatrix} \begin{bmatrix} \Delta f \\ \Delta \delta \\ \Delta E'_q \end{bmatrix}$$
(44)

2024, 9(4s)

e-ISSN: 2468-4376

https://www.jisem-journal.com/

## **Research Article**

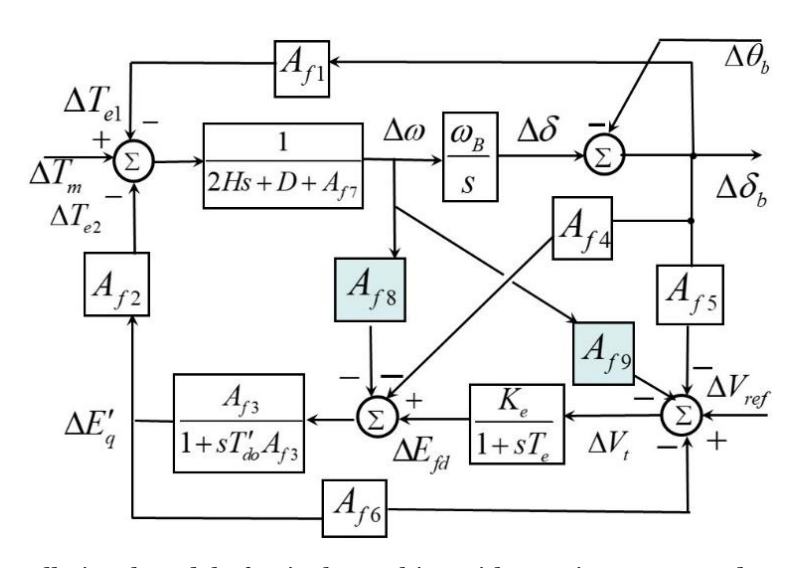


Fig. 4. Small-signal model of a single machine with FDL in a connected network.

Where,

$$A_f = (X_e + \zeta_2 X_{qt}) \zeta_1 X'_{dt} + X_e + X_e^2 X_{qt} X'_{dt} (G_{L0} + G_2) (G_{L0} + G_1)$$

Afterwards  $\Delta I_d$  and  $\Delta I_q$  can be given as:

$$\Delta I_d = C_{f1} \Delta \delta_b + C_{f2} \Delta E_g' + C_{fx} \Delta f \tag{45}$$

$$\Delta I_q = C_{f3} \Delta \delta_b + C_{f4} \Delta E_q' + C_{fb} \Delta f \tag{46}$$

Where,

$$C_{f1} = -E_b A_f^{-1} \begin{bmatrix} (X_e + \zeta_2 X_{qt}) \sin \delta_{b0} \\ + X_e X_{qt} (G_{L0} + G_1) \cos \delta_{b0} \end{bmatrix}$$

$$C_{f2} = -A_f^{-1} \begin{bmatrix} (X_e + \zeta_2 X_{qt}) \zeta_1 + \\ X_e^2 X_{qt} (G_{L0} + G_1) (G_{L0} + G_2) \end{bmatrix}$$

$$C_{f3} = E_b A_f^{-1} \begin{bmatrix} (X_e + \zeta_1 X'_{dt}) \cos \delta_{b0} \\ -X_e X'_{dt} (G_{L0} + G_2) \sin \delta_{b0} \end{bmatrix}$$

$$C_{f4} = X_e^2 A_f^{-1} (G_{L0} + G_2)$$

$$C_{fx} = X_e A_f^{-1} \begin{bmatrix} (X_e + \zeta_2 X_{qt}) F_I \\ -X_e X_{qt} (G_{L0} + G_1) F_R \end{bmatrix}$$

$$C_{fy} = X_e A_f^{-1} \begin{bmatrix} (X_e + \zeta_2 X_{qt}) F_I \\ + (X_e + \zeta_1 X'_{dt}) F_R \end{bmatrix}$$

Next, we develop a small-signal model of a single machine connected to the grid. To this end, the algebraic equations of the stator given in (23) and (24) are linearized as follows:

2024, 9(4s)

e-ISSN: 2468-4376

https://www.jisem-journal.com/

#### **Research Article**

$$\Delta V_a = X_d' \Delta I_d + \Delta E_a' \tag{47}$$

$$\Delta V_d = -X_a \Delta I_a \tag{48}$$

Linearizing (23) and (24), and substituting  $\Delta I_d$  and  $\Delta I_q$  from (45) and (46), we obtain:

$$\Delta V_a = X_d' \left( C_{fx} \Delta f + C_{f1} \Delta \delta_b \right) + \left( 1 + X_d' C_{f2} \right) \Delta E_a' \tag{49}$$

$$\Delta V_d = -X_a \left( C_{f_b} \Delta f + C_{f_3} \Delta \delta_b + C_{f_4} \Delta E_a' \right) \tag{50}$$

Rotor equation in (6) upon linearizing gives:

$$\Delta T_e = \left(E'_{q0} - \left(X_q - X'_d\right)I_{d0}\right)\Delta I_q$$

$$+I_{q0}\Delta E'_q - \left(X_q - X'_d\right)I_{q0}\Delta I_d$$
(51)

Substituting (45) and (46) in (51), we can express  $\Delta T_e$  as:

$$\Delta T_e = A_{f1} \Delta \delta_b + A_{f2} \Delta E_a' + A_{f7} \Delta f \tag{52}$$

Where,

$$A_{f1} = E_{a0}C_{f3} - (X_a - X_d)I_{a0}C_{f1}$$
(53)

$$A_{f2} = E_{q0}C_{f4} + I_{q0} - (X_q - X_d')I_{q0}C_{f2}$$
(54)

$$A_{f7} = E_{q0}C_{fy} - (X_q - X_d')I_{q0}C_{fx}$$
(55)

As,

$$E_{q0} = E'_{q0} - (X_q - X'_d)I_{d0}$$
(56)

Linearizing the equation for the field winding of the  $i^{th}$  machine given in (5), we get the following.

$$T'_{d0} \frac{d\Delta E'_q}{dt} = \Delta E_{fd} - \Delta E'_q + \left(X_d - X'_d\right) \Delta I_d \tag{57}$$

Taking laplace transform of (57) and substituting from (45), we get:

$$1 - (X_d - X_d')C_{f2} + sT_{d0}'\Delta E_q' =$$

$$\Delta E_{fd} + (X_d - X_d')C_{fx}\Delta f + (X_d - X_d')C_{f1}\Delta \delta_b$$

$$(58)$$

which can be further expressed as:

$$(1 + sK_3T'_{d0})\Delta E'_q = A_{f3}\Delta E_{fd} - A_{f3}A_{f8}\Delta f - A_{f3}A_{f4}\Delta \delta_b$$
 (59)

Where,

$$A_{f3} = \frac{1}{1 - (X_d - X_d')C_{f2}} \tag{60}$$

2024, 9(4s)

e-ISSN: 2468-4376

https://www.jisem-journal.com/

## **Research Article**

$$A_{f4} = -(X_d - X_d')C_{f1} \tag{61}$$

$$A_{f8} = -(X_d - X_d')C_{fx}$$
 (62)

The perturbation in the terminal voltage  $(\Delta V_t)$  can be expressed as:

$$\Delta V_{t} = \frac{V_{d0}}{V_{t0}} \Delta V_{d} + \frac{V_{q0}}{V_{t0}} \Delta V_{q}$$
(63)

Substituting from (49) and (50) in (63), we get:

$$\Delta V_t = A_{f5} \Delta \delta_b + A_{f6} \Delta E_q' + A_{f9} \Delta f \tag{64}$$

Where,

$$A_{f5} = -\frac{V_{d0}}{V_{t0}} X_q C_{f3} + \frac{V_{q0}}{V_{t0}} X_d' C_{f1}$$
(65)

$$A_{f6} = -\frac{V_{d0}}{V_{t0}} X_q C_{f4} + \frac{V_{q0}}{V_{t0}} \left( 1 + X_d' C_{f2} \right)$$
 (66)

$$A_{f9} = -\frac{V_{d0}}{V_{t0}} X_q C_{fy} + \frac{V_{q0}}{V_{t0}} X_d' C_{fx}$$
(67)

#### **RESULTS**

## A. IEEE 10-generator 39-bus system

This sub-section outlines the design of a conventional lead-lag power system stabilizer (PSS) for the reference plant model, as depicted in Fig. 4. To validate the proposed plant model, the IEEE 10-machine, 39-bus power system is utilized (see Fig. 5), with relevant data sourced from [41]. The power system model includes a static automatic voltage regulator (AVR) with a high gain of 200 and a time constant of 0.05.

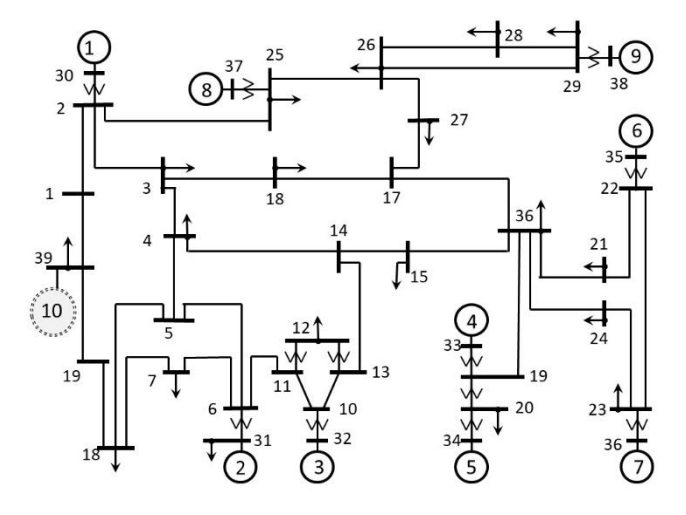


Fig. 5. IEEE 10 generator 39 bus power system model.

2024, 9(4s)

e-ISSN: 2468-4376

https://www.jisem-journal.com/

## **Research Article**

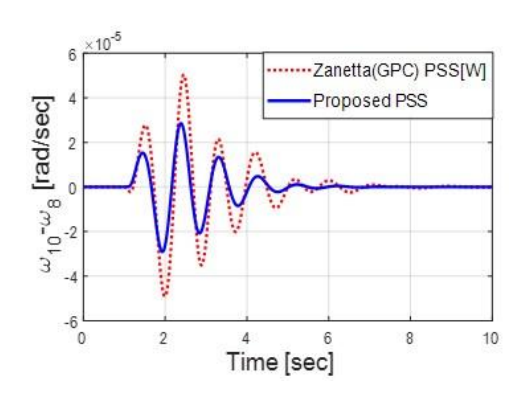


Fig. 6. Slip speed response of Gen-10 w.r.t. Gen-8, wherein a mechanical power change of 0.1 p.u. is given at Gen-8 and Gen-10, Proposed PSS (—) and GPC [W] (-.-).

Fig. 6, shows the slip speed response of Gen-10 w.r.t. Gen8,  $(\omega_{10} - \omega_8)$  when a mechanical power change of 0.1 p.u. and -0.1 p.u. is applied at Gen-8 and Gen-10 respectively.

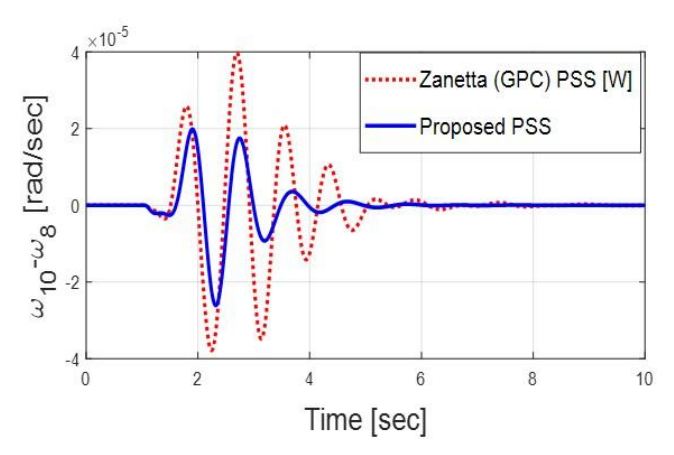


Fig. 7. Slip speed response of Gen-10 w.r.t. Gen-8, following a 0.05 p.u. change in  $V_{ref}$  at Gen-8 and Gen-10, Proposed PSS (—) and GPC [W] (-.-).

Thereafter, in Fig. 7, the slip speed response of Gen-10 w.r.t. Gen-8, ( $\omega_{10}-\omega_8$ ) is given for a 0.05 p.u. and -0.05 p.u. change in  $V_{ref}$  at Gen-8 and Gen-10 respectively.

From Figs. 6 and 7, it is clearly evident that system exhibit superior damping performance with proposed method when compared with [35].

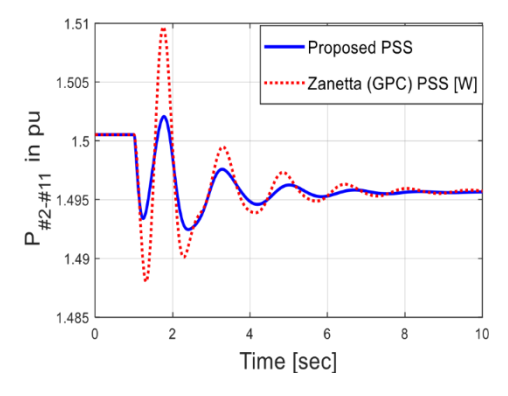


Fig. 8. Tie line real power flow between buses #2-#11, following a 0.05 p.u. mechanical power change in Gen-8 and Gen-10, Proposed PSS (—) and GPC [W] (-.-).

2024, 9(4s)

e-ISSN: 2468-4376

https://www.jisem-journal.com/

#### **Research Article**

Subsequently, Fig. 8 displays the tie line real power flow between buses #2 and #11. To excite the inter-area mode, the real power generation of Gen-8 is increased by 0.05 pu and that of Gen-10 is decreased by 0.05 pu. The results indicate that the PSS designed using FDL effectively dampens real power oscillations.

$$GEP(s) \approx \frac{A_{f2}A_{f3}K_E}{T'_{do}T_EA_{f3}s^2 + (A_{f3}T'_{do} + T_E)s + A_{f3}A_{f6}K_E}$$
(68)

$$H(s) = K_{pss} \frac{1 + sT_1}{1 + sT_2}$$
(69)

The PSS structure is designed for simultaneous tuning of the GPC for the  $k^{th}$  generator and is represented as:

$$H_{GPC}^{k}(s) = \frac{x_{k2}s^{2} + x_{k1}s + x_{k0}}{\left(1 + sT_{k}\right)^{2}} \frac{sT_{\omega}}{1 + sT_{\omega}}$$
(70)

Where,  $k = 1,2,...,n_s$  is the generator number, and  $x_{k2}, x_{k1}, x_{k0} > 0$  are the parameters of  $k^{th}$  stabilizer,  $T_k$  is the time constant,  $T_w$  is the washout time constant. PSS data used in [35] is given in Table VII.

The phase responses of the proposed plant model without frequency-dependent loads (FDLs) closely match those of the transfer function derived from the generalized eigenvalue problem (GEP) presented in Equation (68). However, only the latter transfer function is utilized in this study. A first-order power system stabilizer (PSS) transfer function is employed, as shown in Equation (69). To design the lead-lag phase compensation for both plant models, a similar phase lead is applied. The time constants for the lead-lag phase compensation are provided in Table IV, with the central frequency set to 10 rad/sec.

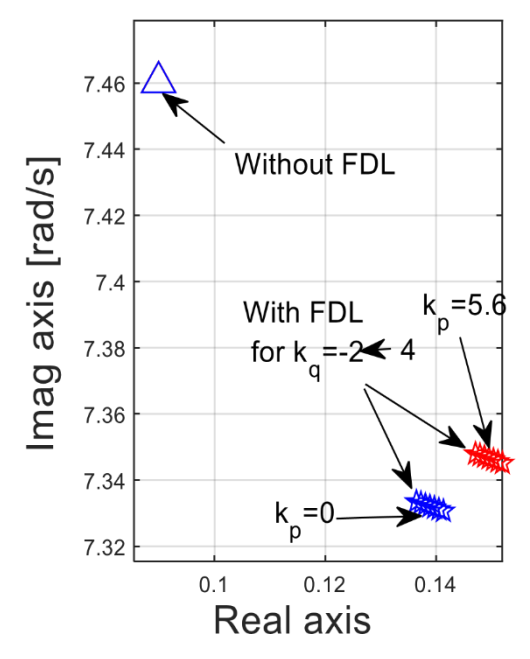


Fig. 9. Rotor modes for the proposed plant model of Gen-9 ( $k_q$ : 4  $\rightarrow$ -2 and  $k_p$ : 0  $\rightarrow$  5.6), with and without FDL.

Finally, rotor modes of Gen-9 are shown in Fig. 9 by varying  $k_p$ : 0 $\rightarrow$ 5.6 and  $k_q$ : 4 $\rightarrow$ -2 with and without FDL. As seen, rotor modes exhibit less damping when  $k_q$ =-2,  $k_p$ =0. Thus, PSS is designed for each generators exhibiting the least damping of system i.e.,  $k_q$ = -2,  $k_p$ = 0. Moduli and angles of the rotor mode pole sensitivities are given in Table III by varying  $k_p$  and  $k_q$  for Gen-7 and Gen-9.

2024, 9(4s)

e-ISSN: 2468-4376

https://www.jisem-journal.com/

# **Research Article**

TABLE III

# MODULI AND ANGLES OF THE ROTOR MODE POLE SENSITIVITIES

	Ge	n-7	Gen-9		
kq	<i>k</i> <sub><i>p</i></sub> = 0	$k_p = 5.6$	<i>k</i> <sub>p</sub> =0	$k_p = 5.6$	
-2.3	0.113∠91.88	0.112∠91.95	0.100∠87.66	0.100∠87.83	
1.8	0.113∠91.89	0.112∠91.97	0.100∠87.37	0.100∠87.81	
4.2	0.112∠91.09	0.112∠91.98	0.100∠ 87.62	0.100∠87.8	

Table III shows rotor mode sensitivities are robust with variation in  $k_p$  and  $k_q$ .

# TABLE IV 39 BUS: PSS DATA WITH FDL [35]

Gen.	Zaneta [35]—		GPC	GC	Proposed	PSS
	xko	x <i>k</i> 1	xko	$\mathbf{K}_k$	$T_1, T_2$	FDL
#30	0.1253	2.5205	13.3687	18.6	0.3, 0.053	43.6
#31	0.0812	1.6273	8.2685	8.7	0.2899, 0.053	20
#32	0.0899	1.797	8.9852	7.9	0.388, 0.0478	10.2
#33	0.0505	1.0457	6.98	7.8	0.5, 0.0365	6.42
#34	0.1423	2.8456	14.2282	11.1	0.33, 0.048	21.6
#35	0.0839	1.6781	8.3905	8.7	0.36, 0.037	9.04
#36	0.066	1.3206	6.6028	6.5	0.356, 0.0389	13.7
#37	0.0583	1.1656	5.8279	5.9	0.412, 0.0349	9.8
#38	0.1232	2.5897	19.2545	15.2	0.352, 0.042	15

# TABLE V39 BUS: OPERATING CONDITIONS.

Conditions	Characteristics
1	Base case
	Lines out: 4-14; 16-17
2	
3	Lines out: 6-11
4	Line out: 3-18; 25-26
5	Load increase of 350 MW

2024, 9(4s)

e-ISSN: 2468-4376

https://www.jisem-journal.com/

# **Research Article**

6	Lines out: 4-14; 25-26; 16-17
	Lines out: 4-14; 25-26; 16-17, 1-39
7	
8	Line out: 21-22
9	Line out: 9-39
10	Load reduction of 20%
11	Load reduction of 30%
12	Load increase of 15%
13	Load increase of 20%
14	Load increase of 50% at 16 and 50% at 21
	and line out: 21-22

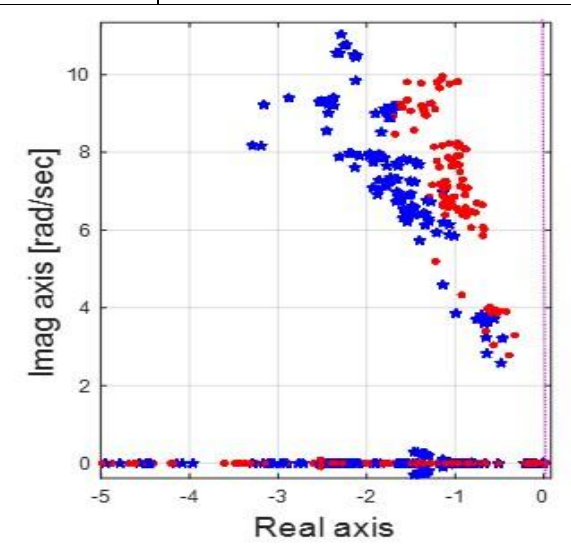


Fig. 10. Eigen values of 39 bus power system for 140 different operatingscenarios. A: proposed PSS, O: GPC PSS. The rotor mode under 14 different operating conditions (see Table V) is shown in Fig. 10. The proposed PSS as seen performs better compared to PSS investigated in [35].

# B. IEEE 16-generator 68-bus system

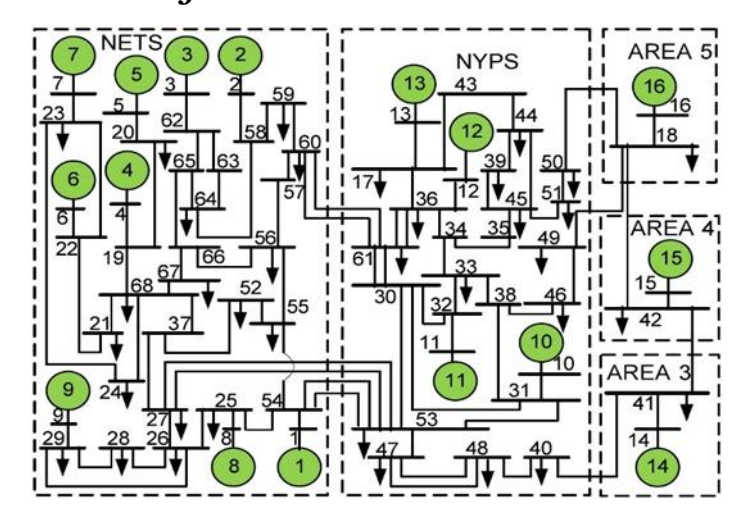


Fig. 11. Line diagram of the 68-bus, power system model.

This subsection discusses an investigation of the IEEE 16- generator 68-bus sub-transient test system, with data

2024, 9(4s)

e-ISSN: 2468-4376

https://www.jisem-journal.com/

#### **Research Article**

sourced from reference [44]. The system comprises of five geograph- ical areas, with generator groups from NETS and NYPS representing two of the areas. The system has a total of eleven local and four inter-area modes in the frequency range of 0.2–2Hz. In order to ensure a fair comparison, each generator in the system is assigned a moderate AVR gain of  $T_d'_O/2T_E$ , where  $T_E = 0.05s$ . The proposed FDL model is used to tunethe PSS for 15% damping, and the corresponding PSS gain values are provided in Table VII.

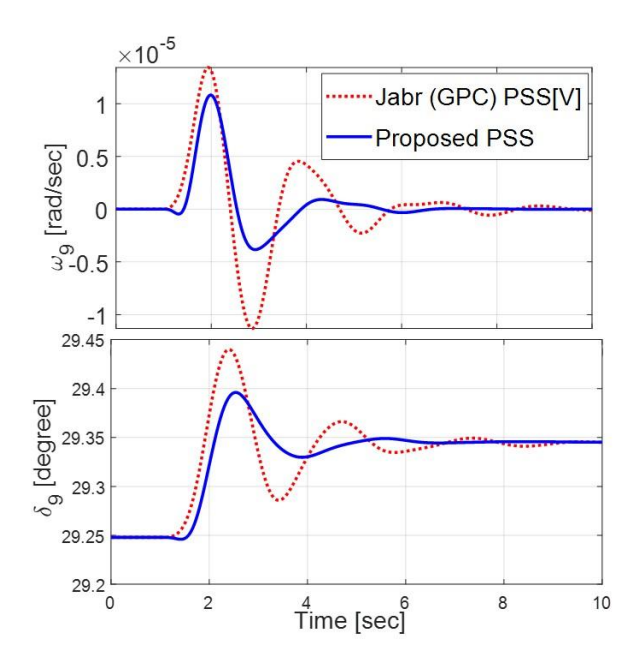


Fig. 12. Slip speed ( $\omega_9$ ) and rotor angle ( $\delta_9$ ) response for a real power change of Gen-9 and Gen-10 by 0.15 pu, Proposed PSS (—) and GPC [V] (-.-).

Fig. 12, shows the response of slip speed ( $\omega_9$ ) and rotor angle ( $\delta_9$ ) for a change in real power input i.e. -0.15 pu for Gen-9 and 0.15 pu for Gen-10. The damping of the rotormode is significantly improved with the proposed PSS when compared to the GPC-PSS technique studied in [36] using sequential conic programming approach.

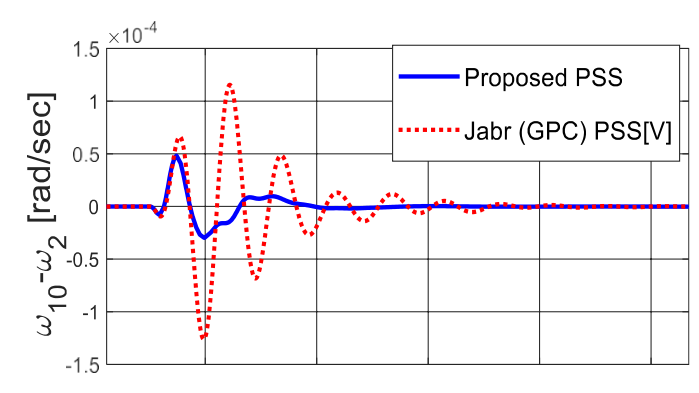


Fig. 13. Slip speed response Gen-2 and Gen-10, following a 0.05 p.u. increase in  $\mathbf{V}_{ref}$  of Gen-5, Proposed PSS (— ) and GPC [V] (-.-).

Next, Fig. 13 presents the slip speed response of Gen-10 w.r.t. Gen-2,  $(\omega_{10} - \omega_2)$  when the reference voltage  $(V_{ref})$  of Gen-5 is increased by 0.05 p.u. for a duration of 100 ms. The proposed PSS is found to provide better damping performance compared to [36].

2024, 9(4s)

e-ISSN: 2468-4376

https://www.jisem-journal.com/

# **Research Article**

# TABLE VI 68 BUS: OPERATING CONDITIONS

Conditions	Characteristics
1	Base case
2	Lines out #53-#54
3	Lines out #60-#61
4	Lines out #27-#53
5	50% constant impedance and 50%constant current
6	50% constant impedance and 50% constant power
7	Lines out #53-#54, #60-#61
8	Lines out #42-#41
9	Lines out #40-#41
10	Lines out #67-#68
11	Load reduction of 30%
12	Load increase of 30%
13	Load reduction of 40%
14	Load increase of 10%

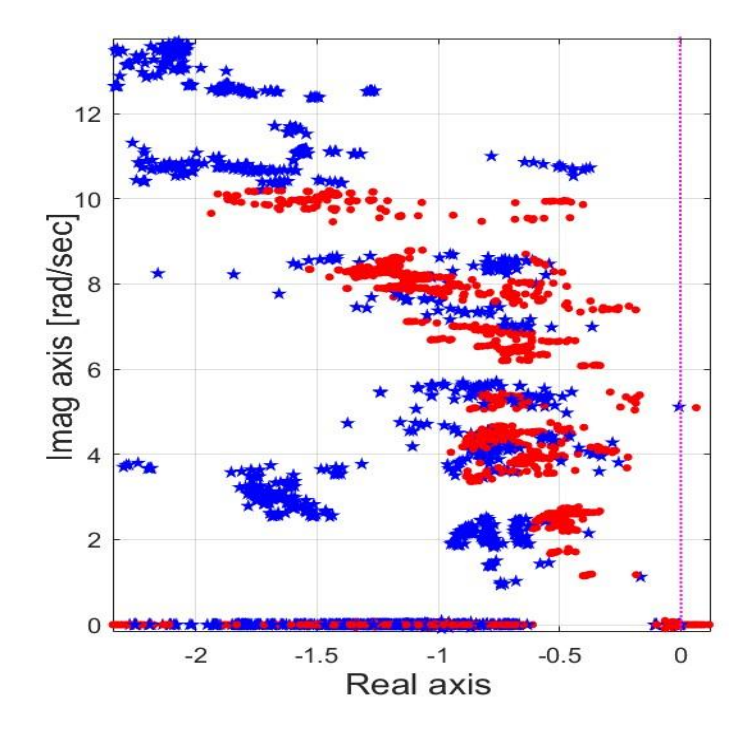


Fig. 14. Eigenvalues of 68 bus power system for 154 different operating scenarios. One of the PSS of generators 1 to 16 are OFFLINE, except critical locations 2, 3, 9, 10, 11. A: proposed PSS, o: GPC PSS [36].

2024, 9(4s)

e-ISSN: 2468-4376

https://www.jisem-journal.com/

## **Research Article**

Finally, Fig. 14 shows the rotor modes for 154 different operating scenarios generated by considering 14 operating conditions as listed in Table VI. In each scenario, one of the PSS of generators 1 to 16 is offline, except for critical locations 2, 3, 9, 10, and 11, resulting in a total of 154 operating scenarios. The proposed PSS is found to make the system more robust compared to the PSS investigated in [36].

TABLE VII
PSS DATA OF 68 BUS POWER SYSTEM FOR FDL

Gen.	Jabr	[36]—	GPC	Proposed PS	S
	xk2	x <i>k</i> 1	xko	$T_1, T_2$	Gain
#1	0.110	2.199	10.999	0.2539, 0.0394	30.7
#2	0.110	2.200	10.999	0.273, 0.0362	12.7
#3	0.110	2.200	10.999	0.273, 0.036	12.6
#4	0.070	1.399	6.999	0.467, 0.034	4.65
#5	0.034	0.911	5.667	0.273, 0.036	20.8
#6	0.090	1.799	8.999	0.273, 0.036	18.3
#7	0.059	1.493	8.999	0.273, 0.036	16.6
#8	0.081	1.624	8.120	0.371, 0.026	16.8
#9	0.110	2.200	10.999	0.316, 0.031	23.2
#10	0.110	2.200	10.999	0.273, 0.036	27.2
#11	0.110	2.199	10.997	0.376, 0.018	6.69
#12	0.110	2.199	10.997	0.273, 0.036	13.2
#13	0.110	2.199	10.999	0.213, 0.046	30.9
#14	0.110	2.199	10.999	0.268, 0.058	28.1
#15	0.110	2.199	10.999	0.371, 0.266	62.6
#16	0.110	2.199	10.999	0.142, 0.069	22.7

## **CONCLUSION**

This paper highlights the potential benefits of FDL connected to the secondary bus of a step-up transformer for improved oscillation damping in a power system. Furthermore, the study presents a conventional lead-lag PSS developed using locally measured data that exhibits better efficacy compared to previous studies by [35] and [36]. The simulation results conducted on, an IEEE 39-bus and 68-bus power system, confirm the effectiveness of the proposed method.

#### APPENDIX I

The state space representation of the system is given as:

$$X = [A]X + [B](\Delta V_{ref} + \Delta V_s)$$

Where, 
$$X^{T} = \left[ \Delta S_{b} \Delta S_{m} \Delta E_{q}' \Delta E_{fd} \right]$$

where, A can be represented as:

$$A = \begin{bmatrix} 0 & \omega_{B} & 0 & 0 \\ -\frac{A_{f1}}{2H} & -\frac{A_{f7} + D}{2H} & -\frac{A_{f2}}{2H} & 0 \\ -\frac{A_{f4}}{T_{cb}'} & -\frac{A_{f3}}{T_{cb}'} & -\frac{1}{A_{f3}T_{cb}'} & \frac{1}{T_{cb}'} \\ -\frac{K_{E}A_{f5}}{T_{E}} & -\frac{K_{E}A_{f9}}{T_{E}} & -\frac{K_{E}A_{f6}}{T_{E}} & -\frac{1}{T_{E}} \end{bmatrix}; B = \begin{bmatrix} 0, 0, 0, \frac{K_{E}}{T_{E}} \end{bmatrix}^{T};$$

2024, 9(4s)

e-ISSN: 2468-4376

https://www.jisem-journal.com/

# **Research Article**

#### APPENDIX II

AVR	Automatic Voltage Regulator
FDL	Frequency Dependent Load
GPC	Gain Phase Compensation

LFEOs Low-Frequency Electromechanical Oscillations

LFOs Low-Frequency Oscillations
PSS Power System Stabilizer
SMIB Single Machine Infinite Bus
WADC Wide Area Damping Controller

### APPENDIX III

LIST OF SYMBOLS			
δ	Rotor angle in radian		
$\omega_{\scriptscriptstyle B},\omega$	Synchronous and rotor speed, in rad/s, respectively		
X	Four-dimensional vector field		
$A_{f1} - A_{f9}$	Linearized SMIB system		
D	Rotor damping co-efficient, in pu.		
$E_q'$	Transient emf due to field flux linkages in pu		
$E_{\it fd}$	Excitation voltage in pu		
Н	Inertia constant in seconds		
$I_q, I_d$	q- and d-axis stator currents, respectively		
$K_{\scriptscriptstyle E},T_{\scriptscriptstyle E}$	AVR gain and time constant		
$m_p, m_q$	Voltage exponent of active and reactive power respectively		
$Q_L, P_L$	Reactive and active power of load bus, respectively		

$Q_S, P_S$	Reactive and active powers of the step-up transformer bus, in pu
$T_{q0}^{\prime},T_{d0}^{\prime}$	q and d-axis transient time constants in second, respectively
$T_m, S_m$	Mechanical torque and slip speed, in pu, respectively
$V_L, I_L$	Voltage and current of load bus, respectively
$X'_q, X'_d$	q- and d-axis transient reactances, in pu
$X_q, X_d$	q-and d-axis steady-state reactances
$X_e, X_t$	Reactance of the transmission line and step-up transformer respectively
$V_r$	Reference voltage magnitude, in pu
$V_{t}$	Terminal voltage magnitude, in pu
$k_{\it pf}$ , $k_{\it qf}$	Frequency sensitivity coefficient for active and reactive power, respectively

# CONFLICT OF INTEREST

The authors declare no conflict of interest.

## **REFRENCES**

- [1] P. Kundur, M. Klein, G. J. Rogers, and M. S. Zywno, "Application of power system stabilizers for enhancement of overall system stability," *IEEE Transactions on Power Systems*, vol. 4, no. 2, pp. 614–626, 1989.
- [2] C. Chung, L. Wang, F. Howell, and P. Kundur, "Generation rescheduling methods to improve power transfer capability constrained by small-signal stability," *IEEE Transactions on Power Systems*, vol. 19, no. 1, pp. 524–530, 2004.

2024, 9(4s)

e-ISSN: 2468-4376

https://www.jisem-journal.com/

#### **Research Article**

- [3] M. J. Gibbard and D. J. Vowles, "Reconciliation of methods of compen-sation for psss in multimachine systems," *IEEE Transactions on Power Systems*, vol. 19, no. 1, pp. 463–472, Feb 2004.
- [4] G. Gurrala and I. Sen, "Power system stabilizers design for intercon- nected power systems," *IEEE Transactions on Power Systems*, vol. 25, no. 2, pp. 1042–1051, May 2010.
- [5] F. J. D. Marco, N. Martins, and J. C. R. Ferraz, "An automatic method for power system stabilizers phase compensation design," *IEEE Transactions on Power Systems*, vol. 28, no. 2, pp. 997–1007, May 2013.
- [6] A. Kumar, "Power system stabilizers design for multimachine power systems using local measurements," *IEEE Tran. Power Syst.*, vol. 31,no. 3, pp. 2163–2171, 2016.
- [7] Z. A. Obaid, M. T. Muhssin, and L. M. Cipcigan, "A model reference-based adaptive pss4b stabilizer for the multi-machines power system," *Electrical Engineering*, vol. 102, no. 1, pp. 349–358, Mar 2020. [Online]. Available: https://doi.org/10.1007/s00202-019-00879-6
- [8] S. Ghosh, "Pss tuning of a radially connected hydro power plant of eastern india using smib model and phase compensation technique," in *2021 9th IEEE International Conference on Power Systems (ICPS)*, 2021, pp. 1–6.
- [9] W. Du, W. Dong, Y. Wang, and H. Wang, "A method to design power system stabilizers in a multi-machine power system based on single-machine infinite-bus system model," *IEEE Transactions on Power Systems*, vol. 36, no. 4, pp. 3475–3486, 2021.
- [10] J. J. Kim and J. H. Park, "A novel structure of a power system stabilizer for microgrids," *Energies*, vol. 14, no. 4, 2021. [Online]. Available: https://www.mdpi.com/1996-1073/14/4/905
- [11] Z. Zhang, W. Qiao, and Q. Hui, "Power system stabilization using energy-dissipating hybrid control," *IEEE Transactions on Power Sys- tems*, vol. 34, no. 1, pp. 215–224, 2019.
- [12] F. Sanniti, G. Tzounas, R. Benato, and F. Milano, "Curvature-based control for low-inertia systems," *IEEE Transactions on Power Systems*, vol. 37, no. 5, pp. 4149–4152, 2022.
- [13] B. Chaudhuri and B. Pal, "Robust damping of multiple swing modes employing global stabilizing signals with a tese," *IEEE Transactions on Power Systems*, vol. 19, no. 1, pp. 499–506, 2004.
- [14] Y. Wan, M. A. A. Murad, M. Liu, and F. Milano, "Voltage frequency control using svc devices coupled with voltage dependent loads," *IEEE Transactions on Power Systems*, vol. 34, no. 2, pp. 1589–1597, 2019.
- [15] R. Xie, I. Kamwa, and C. Y. Chung, "A novel wide-area control strategy for damping of critical frequency oscillations via modulation of active power injections," *IEEE Transactions on Power Systems*, vol. 36, no. 1, pp. 485–494, 2021.
- [16] I. Kamwa, R. Grondin, D. Asber, J. Gingras, and G. Trudel, "Large- scale active-load modulation for angle stability improvement," *IEEE Transactions on Power Systems*, vol. 14, no. 2, pp. 582–590, 1999.
- [17] Trudnowski, Donnelly, and Lightner, "Power-system frequency and stability control using decentralized intelligent loads," in 2005/2006IEEE/PES Transmission and Distribution Conference and Exhibition, 2006, pp. 1453–1459.
- [18] I. Kamwa, R. Grondin, D. Asber, J. Gingras, and G. Trudel, "Active-power stabilizers for multimachine power systems: challenges and prospects," *IEEE Transactions on Power Systems*, vol. 13, no. 4, pp. 1352–1358, 1998.
- [19] F. Wilches-Bernal, R. H. Byrne, and J. Lian, "Damping of inter-area oscillations via modulation of aggregated loads," *IEEE Transactions on Power Systems*, vol. 35, no. 3, pp. 2024–2036, 2020.
- [20] A. Prakash, K. Kumar, and S. K. Parida, "Design of wide-area damping controller based on modulation of active power demand," in *2022 IEEE IAS Global Conference on Emerging Technologies*, 2022, pp. 176–181.
- [21] C. Zhang, D. Ke, Y. Sun, C. Y. Chung, and J. Xu, "Investigations of large-scale voltage-dependent loads for damping inter-area oscillations: Mechanism and robust decentralized control," *IEEE Transactions on Power Systems*, vol. 33, no. 6, pp. 6037–6048, 2018.
- [22] S. Pourmousavi, M. Nehrir, and C. Sastry, "Providing ancillary services through demand response with minimum load manipulation," in *2011 North American Power Symposium*, 2011, pp. 1–6.
- [23] S. B. Crary, "Steady state stability of composite systems," *Electrical Engineering*, vol. 52, no. 11, pp. 787–792, 1933.

2024, 9(4s)

e-ISSN: 2468-4376

https://www.jisem-journal.com/

#### **Research Article**

- [24] C. Concordia and S. Ihara, "Load representation in power system stability studies," *IEEE Transactions on Power Apparatus and Systems*, vol. PAS-101, no. 4, pp. 969–977, 1982.
- [25] J. Milanovic, "Oscillatory interaction between synchronous generator and local voltage-dependent load," *IEE Proceedings Generation, Transmission and Distribution*, vol. 142, pp. 473–480, September 1995.
- [26] S. Wellhöfer, S. Höhn, and M. Luther, "Impact of load modeling on small signal stability investigations," in 2016 IEEE International Conference on Power System Technology (POWERCON), 2016, pp. 1–6.
- [27] L. M. Korunović, J. V. Milanović, S. Z. Djokic, K. Yamashita, S. M. Villanueva, and S. Sterpu, "Recommended parameter values and ranges of most frequently used static load models," *IEEE Transactions on Power Systems*, vol. 33, no. 6, pp. 5923–5934, 2018.
- [28] W. Du, G. Su, H. Wang, and Y. Ji, "Dynamic instability of a power sys-tem caused by aggregation of induction motor loads," *IEEE Transactions on Power Systems*, vol. 34, no. 6, pp. 4361–4369, 2019.
- [29] C. Duan, P. Chakraborty, T. Nishikawa, and A. E. Motter, "Hierarchical power flow control in smart grids: Enhancing rotor angle and frequency stability with demand-side flexibility," *IEEE Transactions on Control of Network Systems*, vol. 8, no. 3, pp. 1046–1058, 2021.
- [30] Q. Zeng, Z. Fan, and L. Jiang, "A local signal based inter-area damping controller via dynamic state estimation approach," in *2022 IEEE Power Energy Society General Meeting (PESGM)*, 2022, pp. 1–5.
- [31] D. D. Simfukwe and B. C. Pal, "Robust and low order power oscillation damper design through polynomial control," *IEEE Transactions on Power Systems*, vol. 28, no. 2, pp. 1599–1608, 2013.
- [32] D. Lam and H. Yee, "A study of frequency responses of generator electrical torques for power system stabilizer design," *IEEE Transactions on Power Systems*, vol. 13, no. 3, pp. 1136–1142, 1998.
- [33] M. Nambu and Y. Ohsawa, "Development of an advanced power systemstabilizer using a strict linearization approach," *IEEE Transactions on Power Systems*, vol. 11, no. 2, pp. 813–818, May 1996.
- [34] M. Garmroodi, D. J. Hill, G. Verbič, and J. Ma, "Impact of load dynamics on electromechanical oscillations of power systems," *IEEE Transactions on Power Systems*, vol. 33, no. 6, pp. 6611–6620, 2018.
- [35] L. C. Zanetta and J. J. D. Cruz, "An incremental approach to the coordinated tuning of power systems stabilizers using mathematical programming," *IEEE Transactions on Power Systems*, vol. 20, no. 2, pp. 895–902, May 2005.
- [36] R. A. Jabr, B. C. Pal, and N. Martins, "A sequential conic program-ming approach for the coordinated and robust design of power system stabilizers," *IEEE Transactions on Power Systems*, vol. 25, no. 3, pp. 1627–1637, Aug 2010.
- [37] M. Klein, G. Rogers, and P. Kundur, "A fundamental study of inter-area oscillations in power systems," *IEEE Transactions on Power Systems*, vol. 6, no. 3, pp. 914–921, 1991.
- [38] I. Kamwa, R. Grondin, and G. Trudel, "Ieee pss2b versus pss4b: the limits of performance of modern power system stabilizers," *IEEE Transactions on Power Systems*, vol. 20, no. 2, pp. 903–915, May 2005.
- [39] E. V. Larsen and D. Swann, "Applying power system stabilizers, parts I, II and III," *IEEE Trans. Power App. Syst.*, vol. PAS-100, No.6, pp. 3017–3046, June 1981.
- [40] P. S. Kundur, Power System Stability and Control. New York: McGraw-Hill, Inc., 1994.
- [41] K. R. Padiyar, Power System Dynamics Stability and Control. John Wiley; Interline Publishing, 1996.
- [42] O. Arguence, B. Raison, and F. Cadoux, "Comments on "impact of load frequency dependence on the ndz and performance of the sfs island-ing detection method"," *IEEE Transactions on Industrial Electronics*, vol. 64, no. 9, pp. 7277–7279, 2017.
- [43] "Load representation for dynamic performance analysis (of power systems)," *IEEE Transactions on Power Systems*, vol. 8, no. 2, pp. 472–482,1993.
- [44] B. Pal and B. Chaudhuri, Robust Control in Power Systems. Springer, 2005.